

Hyper-reduction over nonlinear manifolds for large nonlinear mechanical systems

Shobhit Jain, Paolo Tiso*

November 26, 2021

Institute for Mechanical Systems, ETH Zürich,
Leonhardstrasse 21, 8092 Zürich, Switzerland

Abstract

Common trends in model order reduction of large nonlinear finite-element-discretized systems involve the introduction of a linear mapping into a reduced set of unknowns, followed by Galerkin projection of the governing equations onto a constant reduction basis. Though this reduces the number of unknowns in the system, the computational cost for obtaining the solution could still be high due to the prohibitive computational costs involved in the evaluation of nonlinear terms. Hyper-reduction methods are then seen as a fast way of approximating the nonlinearity in the system of equations. In the finite element context, the energy conserving sampling and weighing (ECSW) method has emerged as a stability and structure-preserving method for hyper-reduction. Classical hyper-reduction techniques, however, are applicable only in the context of linear mappings into the reduction subspace. In this work, we extend the concept of hyper-reduction using ECSW to general nonlinear mappings, while retaining its desirable stability and structure-preserving properties. As a proof of concept, the proposed hyper-reduction technique is demonstrated over models of a flat plate and a realistic wing structure, whose dynamics has been shown to evolve over a nonlinear (quadratic) manifold. An online speed-up of over one thousand times relative to the full system has been obtained for the wing structure using the proposed method, which is higher than its linear counterpart using the ECSW.

Keywords: EECSW; nonlinear manifolds; ECSW; hyper-reduction; model order reduction; structure-preserving; nonlinear dynamics; Galerkin projection

1 Introduction

Model reduction and hyper-reduction

In spite of the ever increasing computational power and digital storage capabilities, reduced-order models (ROM) of Finite Element (FE) discretized systems are a must when complex simulations are needed to support design and optimization activities. Current state-of-the-art ROM techniques are based on a reduced basis approach, i.e., the solution is sought on a *linear*, low-dimensional subspace spanned by a few, carefully selected modes. The resulting residual is then projected onto the same or a different subspace of the same dimension to obtain a well-posed reduced system. When

*Corresponding author. Email: ptiso@ethz.ch

the original system of equations—often referred to as high-fidelity model (HFM)—features symmetric operators, the residual is projected on the same basis used for the approximation of the solution. This procedure is known as the Bubnov-Galerkin projection. The dimensionality reduction is guaranteed by the limited size of the reduction variables as compared to the number of degrees of freedom in the HFM.

When applied to nonlinear systems, projection-based ROMs, while accurate, are not able to deliver significant speedups. This is due to the fact that the computation of the reduced nonlinear terms at each solver iteration scales with the size of the HFM rather than with the one of the reduction subspace. In the case of polynomial nonlinearities, one might consider pre-computing the reduced nonlinear term [18, 17, 16], leading to higher-order tensors. Typically, FE models may also contain rotational DOFs, where the associated nonlinearity cannot be pre-computed and stored in the form of tensors. Furthermore, for high polynomial degrees, the computations with higher-order tensors can become intractable, even more so than the HFM simulations [16]. For such cases, in the most general setting, the above-mentioned scalability issue is successfully alleviated by a range of *hyper-reduction* techniques, which aim at significantly reducing the cost of reduced nonlinear term evaluation by computing them only at few, selected elements or nodes of the FE models, and cheaply approximate the missing information.

The Gappy POD method [19], first introduced for image reconstruction and later applied in dynamical systems [21, 22], was one of the first instances of hyper-reduction. However, as observed by Farhat et al. [5], the term hyper-reduction was introduced much later in [15], where a selection of the integration point in a FE model is performed in a somehow a priori manner. The empirical interpolation method (EIM) [4] approximates a non-affine function using a set of basis functions over a continuous, bounded domain, and hence finds applications for reduced basis representations of parameterized partial differential equations (PDEs). The discrete empirical interpolation method (DEIM) [1] achieves this on a spatially discretized domain. For FE applications, the unassembled DEIM or UDEIM [2] was shown to be more efficient, where the unassembled element-level nonlinear force vector is used in the DEIM algorithm to return a small set of elements (instead of nodes) over which the nonlinearity is evaluated. For conservative/port-Hamiltonian systems, however, the DEIM (or UDEIM) leads to a loss of numerical stability during time integration. Though a symmetrized version of DEIM has been proposed recently [3] to avoid this issue, its potential for FE-based applications remains unexplored. To this end, the energy-conserving sampling and weighting (ECSW) hyper-reduction method [5] is remarkable. The ECSW method directly approximates the *reduced* nonlinear term and is particularly well-suited for FE-based structural dynamics applications, as it preserves the symmetry of the operators involved and leads to numerical stability.

The main idea of ECSW is simple yet powerful: only few elements are interrogated to compute the nonlinear forces, and weights (obtained using training) are attached to them to match the virtual work done by their full counterparts onto virtual displacements given by the linear reduction basis vectors. Albeit being efficient and relevant for FE-based mechanical systems, the ECSW method, by construction, is limited to perform hyper-reduction of systems over strictly *linear* subspaces. To the best of the authors' knowledge, this limitation is shared by all other hyper-reduction techniques in the literature, as well.

Nonlinear manifolds in model reduction

It is quite natural, however, for the dynamics of general nonlinear systems to evolve on inherently nonlinear manifolds, and not over linear subspaces (cf. [20] for a discussion). Often, a nonlinear manifold relevant for system dynamics may not be embeddable in a low-dimensional linear subspace. It is then easy to see that the linear-mapping-based ROM would either fail to capture the system response, or require frequent basis-updates (online) to account for the nonlinearity, making the reduction process cumbersome and possibly redundant due to high computational costs in setting up such a ROM. Many methods allow for model reduction using attracting nonlinear manifolds in nonlinear dynamical systems – from a theoretical, as well as a data-driven, statistical perspective.

The approximate inertial manifold (AIM) provides an approximation of the solution of a PDE over sufficiently long time scales, using the theory of inertial manifolds. This is done by enslaving the amplitudes of fast modes in the system as a smooth graph over the amplitudes of a few selected modes while assuming that the corresponding inertial forces are not excited (see [25, 6], for instance). The so called static condensation approach (cf. [17]) achieves the same objective without the projection of the governing equations on to eigenfunctions. This is usually done for systems exhibiting a dichotomy of unknowns, such as the axial (in-plane) and transverse (out-of-plane) unknowns in a beam or a plate. From the perspective of nonlinear dynamics, a good overview of nonlinear model reduction techniques can be found in [24] and the references therein.

Over the past decade or so, the use of nonlinear manifolds in model reduction has received a significant boost by many data-driven techniques, broadly referred to as *nonlinear dimensionality reduction* (NLDR) or *manifold learning*, see [14], for instance. These techniques aim at constructing low dimensional manifolds from high-dimensional data snapshots. In a ROM perspective, these snapshots may be extracted from simulations of the underlying HFM, and the chosen NLDR is deemed to provide a nonlinear mapping with the required smoothness [9]. In essence, these methods provide a nonlinear generalization of the Proper Orthogonal Decomposition (POD), a well-known technique which delivers an optimal linear subspace for the dimensionality reduction.

The use of nonlinear manifolds in model reduction is expected to not only further reduce the size of the ROM in contrast to its linear mapping counterpart, but also shed light on the underlying system behaviour. This is, especially, true for the case of thin walled structures, which exhibit a time scale separation between slow, out-of-plane; and fast, in-plane dynamics. The fast dynamics in such systems can often be enslaved statically to the slow one, in a nonlinear fashion [8]. Recent efforts [11, 12] have shown that the geometrically nonlinear dynamics of structures, characterized by bending-stretching coupling (as for instance, thin walled components) can be effectively captured using a quadratic manifold (QM), constructed using model properties rather than HFM snapshots.

Our contribution

The nonlinear-manifold-based ROMs are usually obtained by projecting the HFM on the tangent space of the manifold, in a virtual work sense. This generates configuration-dependent inertial terms for the ROM in addition to the already existing projected nonlinear terms. For general nonlinear systems, the evaluation and projection of the nonlinearity remains a bottleneck for computations, much like the linear mapping counterpart. As discussed above, the state-of-the-art hyper-reduction techniques allow for fast approximation of the (projected) nonlinearity in the case of linear-mapping-based ROMs. This functionality, however, has been missing in the context of nonlinear-manifold-based ROMs.

In this contribution, we generalize the application of the ECSW hyper-reduction method to nonlinear-manifold-based ROMs. This work is essentially inspired from the ideas in the seminal work of Farhat et al. [5, 7], where ECSW method was introduced in the context of linear mappings. Following similar lines as in [7], we further show that our extension of the ECSW (named hereafter as *extended* ECSW: EECSW) preserves the Lagrangian structure associated with the Hamilton's principle. A natural consequence of this property is the numerical stability during hyper-reduction, as shown in [7]. The proposed method is tested, first on an academically simple example, and then on a realistic model of a wing using the recently proposed QM for reduction. Our numerical results indicate that better speed ups can be achieved, as compared to the ones obtained with a linear POD subspace reduction of comparable accuracy equipped with ECSW. Remarkably, EECSW selects less elements for the hyper-reduction as compared to its linear counterpart, and more than compensates the extra computational costs associated to the configuration dependent inertial terms, which are not present in the case of linear subspace reduction.

This paper is organized as follows. The concept of projection based ROM on nonlinear mappings is briefly reviewed in Section 2. The extension of ECSW for nonlinear mappings is the tackled in Section 3, where also the preservation of the Lagrangian structure of the thus-obtained ROM is

shown. Numerical results showing the effectiveness of the method are reported in Section 4, and finally, the conclusions are given in Section 5.

2 Model reduction using nonlinear mappings

The partial differential equations (PDEs) for momentum balance in a structural continuum are first FE discretized along the spatial dimensions to obtain a system of second-order ordinary differential equations (ODEs). Along with the initial conditions for generalized displacements and velocities, these ODEs govern the response of the underlying structure. More specifically, this response can be described by the solution to an initial value problem (IVP) of the following form:

$$\begin{aligned} \mathbf{M}\ddot{\mathbf{u}}(t) + \mathbf{C}\dot{\mathbf{u}}(t) + \mathbf{f}(\mathbf{u}(t)) &= \mathbf{g}(t), \\ \mathbf{u}(t_0) = \mathbf{u}_0, \dot{\mathbf{u}}(t_0) &= \mathbf{v}_0, \end{aligned} \quad (1)$$

where the solution $\mathbf{u}(t) \in \mathbb{R}^n$ is a high-dimensional generalized displacement vector, $\mathbf{M} \in \mathbb{R}^{n \times n}$ is the mass matrix; $\mathbf{C} \in \mathbb{R}^{n \times n}$ is the damping matrix; $\mathbf{f} : \mathbb{R}^n \mapsto \mathbb{R}^n$ gives the nonlinear elastic internal force as a function of the displacement \mathbf{u} of the structure; and $\mathbf{g}(t) \in \mathbb{R}^n$ is the time dependent external load vector. The system (1), referred to as the high-fidelity model (HFM), exhibits prohibitive computational costs for large values of the dimension n of the system. The classical notion of model reduction aims to reduce this dimensionality by introducing a linear mapping on to a suitable low-dimensional invariant subspace. However, as discussed in the Introduction, more recent advances in model reduction allow for the detection of system dynamics, evolving over nonlinear manifolds. The idea of a projection-based reduced-order model using nonlinear mappings was presented in [11], using a nonlinear mapping such as

$$\mathbf{u}(t) \approx \mathbf{\Gamma}(\mathbf{q}(t)), \quad (2)$$

where $\mathbf{\Gamma} : \mathbb{R}^m \mapsto \mathbb{R}^n$ is the nonlinear mapping function. In general the mapping (2), when substituted into the governing equations (1), results in a non-zero residual \mathbf{r} as

$$\mathbf{M}\ddot{\mathbf{\Gamma}}(\mathbf{q}(t)) + \mathbf{C}\dot{\mathbf{\Gamma}}(\mathbf{q}(t)) + \mathbf{f}(\mathbf{\Gamma}(\mathbf{q}(t))) - \mathbf{g}(t) = \mathbf{r}.$$

The virtual work principle for a kinematically admissible displacement, $\delta \mathbf{u} = \frac{\partial \mathbf{\Gamma}(\mathbf{q})}{\partial \mathbf{q}} \delta \mathbf{q}$, over the nonlinear manifold leads to

$$\begin{aligned} \mathbf{r} \cdot \delta \mathbf{u} &= 0 \\ \implies \left[\mathbf{M}\ddot{\mathbf{\Gamma}}(\mathbf{q}(t)) + \mathbf{C}\dot{\mathbf{\Gamma}}(\mathbf{q}(t)) + \mathbf{f}(\mathbf{\Gamma}(\mathbf{q}(t))) \right] \cdot \delta \mathbf{u} &= \mathbf{g}(t) \cdot \delta \mathbf{u}. \end{aligned}$$

Physically, this means that the residual force is orthogonal to the tangent space of the manifold. This gives the corresponding reduced-order model as

$$\mathbf{P}_{\mathbf{\Gamma}}^T \left[\mathbf{M}\ddot{\mathbf{\Gamma}}(\mathbf{q}(t)) + \mathbf{C}\dot{\mathbf{\Gamma}}(\mathbf{q}(t)) + \mathbf{f}(\mathbf{\Gamma}(\mathbf{q}(t))) \right] = \mathbf{P}_{\mathbf{\Gamma}}^T \mathbf{g}(t), \quad (3)$$

where $\mathbf{P}_{\mathbf{\Gamma}} = \frac{\partial \mathbf{\Gamma}(\mathbf{q})}{\partial \mathbf{q}} \in \mathbb{R}^{n \times m}$ represents the tangent space of the nonlinear manifold in which the system dynamics is expected to evolve. The acceleration and velocity vectors over the manifold can be evaluated using the chain rule as

$$\begin{aligned} \dot{\mathbf{\Gamma}}(\mathbf{q}(t)) &= \frac{d}{dt} \mathbf{\Gamma}(\mathbf{q}(t)) = \frac{\partial \mathbf{\Gamma}(\mathbf{q})}{\partial \mathbf{q}} \cdot \dot{\mathbf{q}}, \\ \ddot{\mathbf{\Gamma}}(\mathbf{q}(t)) &= \frac{d}{dt} \dot{\mathbf{\Gamma}}(\mathbf{q}(t)) = \frac{\partial \mathbf{\Gamma}(\mathbf{q})}{\partial \mathbf{q}} \cdot \ddot{\mathbf{q}} + \left[\frac{\partial^2 \mathbf{\Gamma}(\mathbf{q})}{\partial \mathbf{q} \partial \mathbf{q}} \cdot \dot{\mathbf{q}} \right] \cdot \dot{\mathbf{q}}. \end{aligned}$$

Using the above relations, (3) can also be expressed as

$$\mathbf{M}_r(\mathbf{q}) \ddot{\mathbf{q}} + \mathbf{C}_r(\mathbf{q}, \dot{\mathbf{q}}) \dot{\mathbf{q}} + \mathbf{f}_r(\mathbf{q}) = \mathbf{P}_{\mathbf{\Gamma}}^T \mathbf{g}(t), \quad (4)$$

where $\mathbf{M}_r(\mathbf{q}) = \mathbf{P}_\Gamma^T \mathbf{M} \mathbf{P}_\Gamma$, $\mathbf{C}_r(\mathbf{q}, \dot{\mathbf{q}}) = \mathbf{P}_\Gamma^T \mathbf{C} \mathbf{P}_\Gamma + \mathbf{P}_\Gamma^T \mathbf{M} \left(\frac{\partial^2 \Gamma(\mathbf{q})}{\partial \mathbf{q} \partial \dot{\mathbf{q}}} \cdot \dot{\mathbf{q}} \right)$ and $\mathbf{f}_r(\mathbf{q}) = \mathbf{P}_\Gamma^T \mathbf{f}(\Gamma(\mathbf{q}))$.

Note that for Γ being a linear function, such that $\Gamma(\mathbf{q}) = \mathbf{V} \mathbf{q}$ (for some $\mathbf{V} \in \mathbb{R}^{n \times m}$ spanning a suitable low dimensional subspace), the ROM in (3) reduces to the familiar Galerkin-projection-based ROMs as

$$\mathbf{V}^T \mathbf{M} \mathbf{V} \ddot{\mathbf{q}}(t) + \mathbf{V}^T \mathbf{C} \mathbf{V} \dot{\mathbf{q}}(t) + \mathbf{V}^T \mathbf{f}(\mathbf{V} \mathbf{q}(t)) = \mathbf{V}^T \mathbf{g}(t). \quad (5)$$

During time integration - usually referred to as *online phase* - of (5), the computational cost associated to the evaluation of the linear terms in (5) scales only with the number of reduced variables m , since the corresponding reduced operators can be pre-computed *offline*. However, this is not the case for the computation of the reduced nonlinear term $\mathbf{V}^T \mathbf{f}(\mathbf{V} \mathbf{q}(t))$. Specifically, for FE-based applications, this evaluation is usually carried out *online*, in the following manner:

$$\hat{\mathbf{f}}(\mathbf{q}) := \mathbf{V}^T \mathbf{f}(\mathbf{V} \mathbf{q}) = \sum_{e=1}^{n_e} \mathbf{V}_e^T \mathbf{f}_e(\mathbf{V}_e \mathbf{q}), \quad (6)$$

where $\mathbf{f}_e(\mathbf{u}_e) \in \mathbb{R}^{N_e}$ is the contribution of the element e towards the vector $\mathbf{f}(\mathbf{u})$ (N_e being the number of DOFs for the element e), \mathbf{V}_e is the restriction of \mathbf{V} to the rows indexed by the DOFs corresponding to e , and n_e is the total number of elements in the structure. It is then easy to see from (6), that the cost associated to the computation of the reduced nonlinear force $\hat{\mathbf{f}}(\mathbf{q})$ scales linearly with the total number of elements n_e in the structure, which is potentially high for large systems. Thus, despite the reduction in dimensionality achieved in (5), the evaluation of the reduced nonlinear term $\hat{\mathbf{f}}(\mathbf{q})$ emerges as a new bottleneck for the fast prediction of system response using the ROM (5). Similar conclusions regarding computational bottlenecks hold for the nonlinear-reduction-based ROM (3), as well.

3 Hyper-reduction and Extended ECSW

Hyper-reduction techniques help mitigate the above-stated high computational costs by approximation of the reduced-nonlinear term in a computationally affordable manner. As discussed in the Introduction, the ECSW [5] is a remarkable method for hyper-reduction of linear-mapping-based ROMs such as that in (5). After briefly summarizing ECSW, we propose here an extension to ECSW, which facilitates hyper-reduction of nonlinear-manifold-based ROM, such as in (3). Much like ECSW, we further show in that the proposed extended ECSW (EECSW) is numerically stable due to preservation of the Lagrangian structure associated to the underlying mechanical system.

Analogous to (6), the projected nonlinear force (possibly a combination of inertial, damping or elastic forces) in the ROM (3) can be expressed as a summation of the element-level contributions as

$$\mathbf{h}_r(\mathbf{q}, \dot{\mathbf{q}}, \ddot{\mathbf{q}}) = \mathbf{P}_\Gamma^T \mathbf{h} \left(\Gamma(\mathbf{q}), \dot{\Gamma}(\mathbf{q}), \ddot{\Gamma}(\mathbf{q}) \right) = \sum_{e=1}^{n_e} (\mathbf{P}_\Gamma(\mathbf{q}))_e^T \mathbf{h}_e \left(\Gamma_e(\mathbf{q}), \dot{\Gamma}_e(\mathbf{q}), \ddot{\Gamma}_e(\mathbf{q}) \right), \quad (7)$$

where $\mathbf{h}_r(\mathbf{q}, \dot{\mathbf{q}}, \ddot{\mathbf{q}})$ is the part of the ROM (3) which is potentially unaffordable to compute (cost scales with n or n_e), \mathbf{h} is its full counterpart, with the \mathbf{h}_e having the usual meaning for the element-level contribution from the element e . One easily observable distinction of EECSW from its linear mapping counterpart is that one can precompute the reduced linear operators in the hyper-reduced model. Due to the nonlinear mapping and projection on the tangent space, we see that EECSW doesn't feature reduced-linear operators, even for the linear mass, stiffness and damping matrices in the HFM. Thus, in principle, one could include all the terms on the left hand of (3) in \mathbf{h}_r , i.e.,

$$\mathbf{h}_r(\mathbf{q}, \dot{\mathbf{q}}, \ddot{\mathbf{q}}) = \mathbf{P}_\Gamma^T \left[\mathbf{M} \ddot{\Gamma}(\mathbf{q}(t)) + \mathbf{C} \dot{\Gamma}(\mathbf{q}(t)) + \mathbf{f}(\Gamma(\mathbf{q}(t))) \right].$$

The summation in (7) can be approximated as

$$\text{(EECSW)} \quad \mathbf{h}_r(\mathbf{q}, \dot{\mathbf{q}}, \ddot{\mathbf{q}}) \approx \tilde{\mathbf{h}}_r(\mathbf{q}, \dot{\mathbf{q}}, \ddot{\mathbf{q}}) = \sum_{e \in E} \xi_e (\mathbf{P}_\Gamma(\mathbf{q}))_e^T \mathbf{h}_e \left(\Gamma_e(\mathbf{q}), \dot{\Gamma}_e(\mathbf{q}), \ddot{\Gamma}_e(\mathbf{q}) \right), \quad (8)$$

where $\xi_e \in \mathbb{R}^+$ is a positive weight given to every element $e \in E$. These weights would be smartly chosen using *training* to ensure a good approximation of the original sum over all n_e elements. Clearly, the evaluation of $\tilde{\mathbf{h}}_r$ in (8) comes at a fraction of the computational cost associated to (7), for $|E| \ll n_e$.

It is easy to see that this idea is a straight-forward generalization of ECSW to nonlinear-manifold-based ROMs with projection to the tangent space, as given in (3). Indeed, for $\mathbf{\Gamma}(\mathbf{q}) = \mathbf{V}\mathbf{q}$, hyper-reduction of ROM (5) results in the approximation of the projected internal force in (6) as

$$\hat{\mathbf{f}}(\mathbf{q}) \approx \tilde{\mathbf{f}}(\mathbf{q}) = \sum_{e \in E} \xi_e \mathbf{V}_e^T \mathbf{f}_e(\mathbf{V}_e \mathbf{q}), \quad (9)$$

which is same as the expression one would obtain from the direct application of ECSW, as well.

3.1 Element weight selection

The elements and weights are determined to approximate virtual work over chosen training sets which generally come from full solution run(s). We assume that $\{\mathbf{u}^{(i)}, \dot{\mathbf{u}}^{(i)}, \ddot{\mathbf{u}}^{(i)}\}$, $i \in \{1, \dots, n_t\}$ represents a set of available training vectors. If the solution to the HFM, indeed, evolves over a nonlinear manifold as given by (2), then we must be able to find reduced unknowns $\{\mathbf{q}^{(i)}, \dot{\mathbf{q}}^{(i)}, \ddot{\mathbf{q}}^{(i)}\}$ ¹ such that

$$\left. \begin{aligned} \mathbf{u}^{(i)} &\approx \mathbf{\Gamma}(\mathbf{q}^{(i)}) \\ \dot{\mathbf{u}}^{(i)} &\approx \mathbf{P}_{\mathbf{\Gamma}}(\mathbf{q}^{(i)}) \dot{\mathbf{q}}^{(i)} \\ \ddot{\mathbf{u}}^{(i)} &\approx \mathbf{P}_{\mathbf{\Gamma}}^T(\mathbf{q}^{(i)}) \ddot{\mathbf{q}}^{(i)} + \left[\frac{\partial^2 \mathbf{\Gamma}(\mathbf{q})}{\partial \mathbf{q} \partial \mathbf{q}} \Big|_{\mathbf{q}=\mathbf{q}^{(i)}} \cdot \dot{\mathbf{q}}^{(i)} \right] \cdot \dot{\mathbf{q}}^{(i)} \end{aligned} \right\} \forall i \in \{1, \dots, n_t\}, \quad (10)$$

As will be clear later in this section, the optimal elements and weights corresponding to a reduced mesh needs the set of reduced vectors $\{\mathbf{q}^{(i)}, \dot{\mathbf{q}}^{(i)}, \ddot{\mathbf{q}}^{(i)}\}$ during the training stage. In case these are available from a previous ROM simulation, these would be directly useful. However, if not, the nonlinear system of algebraic equations (10) can be solved for the reduced training vectors $\mathbf{q}^{(i)}$, $\dot{\mathbf{q}}^{(i)}$, and $\ddot{\mathbf{q}}^{(i)}$ in a sequential manner. This system is potentially under-constrained ($n_t < n$ usually) and, hence, the sought $\mathbf{q}^{(i)}$ can be obtained from the solution to a nonlinear least-squares problem as

$$\mathbf{q}^{(i)} = \arg \min_{\mathbf{q} \in \mathbb{R}^m} \left\| \mathbf{\Gamma}(\mathbf{q}) - \mathbf{u}^{(i)} \right\|_2^2. \quad (11)$$

Once $\mathbf{q}^{(i)}$ is obtained, the second equation in (10) can be solved in a least squares sense for $\dot{\mathbf{q}}^{(i)}$ as

$$\dot{\mathbf{q}}^{(i)} = \left[\mathbf{P}_{\mathbf{\Gamma}}^T(\mathbf{q}^{(i)}) \mathbf{P}_{\mathbf{\Gamma}}(\mathbf{q}^{(i)}) \right]^{-1} \mathbf{P}_{\mathbf{\Gamma}}^T(\mathbf{q}^{(i)}) \dot{\mathbf{u}}^{(i)}.$$

Finally, one can obtain the corresponding reduced accelerations as

$$\ddot{\mathbf{q}}^{(i)} = \left[\mathbf{P}_{\mathbf{\Gamma}}^T(\mathbf{q}^{(i)}) \mathbf{P}_{\mathbf{\Gamma}}(\mathbf{q}^{(i)}) \right]^{-1} \mathbf{P}_{\mathbf{\Gamma}}^T(\mathbf{q}^{(i)}) \left(\ddot{\mathbf{u}}^{(i)} - \left[\frac{\partial^2 \mathbf{\Gamma}(\mathbf{q})}{\partial \mathbf{q} \partial \mathbf{q}} \Big|_{\mathbf{q}=\mathbf{q}^{(i)}} \cdot \dot{\mathbf{q}}^{(i)} \right] \cdot \dot{\mathbf{q}}^{(i)} \right).$$

¹Note that the ROM (4) can be expressed as:
 $\ddot{\mathbf{q}} + \mathbf{M}_r^{-1}(\mathbf{q}) \mathbf{C}_r(\mathbf{q}, \dot{\mathbf{q}}) \dot{\mathbf{q}} + \mathbf{M}_r^{-1}(\mathbf{q}) \mathbf{f}_r(\mathbf{q}) = \mathbf{M}_r^{-1}(\mathbf{q}) \mathbf{P}_{\mathbf{\Gamma}}^T \mathbf{g}(t)$,
and by doing so, the inertial terms in the ROM become linear and require no hyper-reduction. This would also avoid the need for the acceleration training vectors $\ddot{\mathbf{u}}^{(i)}$ or $\ddot{\mathbf{q}}^{(i)}$, as is the case in ECSW. Nonetheless, we treat hyper-reduction and training in the straight-forward and general setting of (3) where the inertial terms may be hyper-reduced and acceleration training may also be performed.

Note that for $\mathbf{\Gamma}$ being a linear function, such as $\mathbf{\Gamma}(\mathbf{q}) = \mathbf{V}\mathbf{q}$, the system (11) reduces to the familiar least squares solution of (10), available in closed form as

$$\begin{aligned}\mathbf{q}^{(i)} &= (\mathbf{V}^T \mathbf{V})^{-1} \mathbf{V}^T \mathbf{u}^{(i)}, \\ \dot{\mathbf{q}}^{(i)} &= (\mathbf{V}^T \mathbf{V})^{-1} \mathbf{V}^T \dot{\mathbf{u}}^{(i)}, \\ \ddot{\mathbf{q}}^{(i)} &= (\mathbf{V}^T \mathbf{V})^{-1} \mathbf{V}^T \ddot{\mathbf{u}}^{(i)}.\end{aligned}$$

For general nonlinear mappings, however, iterative methods would be needed to solve (11). Starting with an initial guess $\mathbf{q}_0^{(i)}$ for the solution, one such simple iterative procedure is the gradient-descent method (cf. [13] for a review of methods for nonlinear least squares problems), and can be formulated as follows:

$$\begin{aligned}r(\mathbf{q}_k^{(i)}) &:= \left\| \mathbf{\Gamma}(\mathbf{q}_k^{(i)}) - \mathbf{u}^{(i)} \right\|_2^2, \\ \mathbf{q}_{k+1}^{(i)} &= \mathbf{q}_k^{(i)} - \gamma_k \nabla r(\mathbf{q}_k^{(i)}),\end{aligned}\tag{12}$$

where γ_k is the well-known descent rate, which should be chosen small enough to facilitate smooth decay to the local minimum of r , and the ∇r is the gradient of r , obtained using the configuration-dependent tangent space $\mathbf{P}_{\mathbf{\Gamma}}^T$ of the nonlinear manifold as

$$\nabla r(\mathbf{q}_k^{(i)}) = \mathbf{P}_{\mathbf{\Gamma}}^T(\mathbf{q}_k^{(i)}) \left(\mathbf{\Gamma}(\mathbf{q}_k^{(i)}) - \mathbf{u}^{(i)} \right).$$

Once the reduced training vectors $\{\mathbf{q}^{(i)}, \dot{\mathbf{q}}^{(i)}, \ddot{\mathbf{q}}^{(i)}\}$ are obtained, the element level contribution of projected internal force for each of the training vectors can be assembled in a matrix \mathbf{G} as follows:

$$\begin{aligned}\mathbf{G} &= \begin{bmatrix} \mathbf{g}_{11} & \cdots & \mathbf{g}_{1n_e} \\ \vdots & \ddots & \vdots \\ \mathbf{g}_{n_t 1} & \cdots & \mathbf{g}_{n_t n_e} \end{bmatrix} \in \mathbb{R}^{mn_t \times n_e}, \quad \mathbf{b} = \begin{bmatrix} \mathbf{b}_1 \\ \vdots \\ \mathbf{b}_{n_t} \end{bmatrix} \in \mathbb{R}^{mn_t}, \\ \mathbf{g}_{ie} &= \left(\mathbf{P}_{\mathbf{\Gamma}}(\mathbf{q}^{(i)}) \right)_e^T \mathbf{h}_e \left(\mathbf{\Gamma}_e(\mathbf{q}^{(i)}), \dot{\mathbf{\Gamma}}_e(\mathbf{q}^{(i)}), \ddot{\mathbf{\Gamma}}_e(\mathbf{q}^{(i)}) \right), \quad \mathbf{b}_i = \mathbf{f}_r(\mathbf{q}^{(i)}) = \sum_{e=1}^{n_e} \mathbf{g}_{ie} \\ &\forall i \in \{1, \dots, n_t\}, \quad e \in \{1, \dots, n_e\}.\end{aligned}\tag{13}$$

Analogous to ECSW, the set of elements and weights is then obtained by a sparse solution to the following non-negative least-squares (NNLS) problem

$$(P1) : \zeta = \arg \min_{\zeta \in \mathbb{R}^{n_e}, \zeta \geq \mathbf{0}} \|\mathbf{G}\zeta - \mathbf{b}\|_2^2,\tag{14}$$

A sparse solution to (P1) returns a sparse vector ζ , the non-zero entries of which form the reduced mesh Z used in (9) as

$$Z = \{e : \zeta_e > 0\}.$$

An optimally sparse solution to (P1) is NP-hard to obtain. However, a greedy-approach-based algorithm [10], which finds a sub-optimal solution, has been found to deliver an effective reduced mesh Z [5]. For the sake of completeness, we have included its pseudo-code in Algorithm 1. More recent work [23] proposes and discusses different alternatives to accelerate the sampling procedure during hyper-reduction.

Algorithm 1 Training for EECSW

Input: $\{\mathbf{u}^{(i)}\}$, $i \in \{1, \dots, n_t\}$, τ (sparse NNLS tolerance)**Output:** $\boldsymbol{\xi} \in \mathbb{R}^{n_e}$ sparse, $E \subset \{1, \dots, n_e\}$

```
1: for  $i \leftarrow 1$  to  $n_t$  do
2:    $\mathbf{q}^{(i)} \leftarrow \text{LSQNLIN}(\mathbf{u}^{(i)})$   $\triangleright$  LSQNLIN: solves the nonlinear least squares problem (11), e.g.,
   using gradient descent method (12)
3: end for
4:  $[\mathbf{G}, \mathbf{b}] \leftarrow \text{Construct\_G\_b}(\{\mathbf{q}^{(i)}\}_1^{n_t})$   $\triangleright$  Construct_G_b: assembles  $\mathbf{G}, \mathbf{b}$ , as given by (13)
5:  $E \leftarrow \emptyset, Z \leftarrow \{1, \dots, n_e\}, \boldsymbol{\xi} \leftarrow \mathbf{0} \in \mathbb{R}^{n_e}$ 
6: while  $\|\mathbf{G}\boldsymbol{\xi} - \mathbf{b}\|_2 > \tau\|\mathbf{b}\|_2$  do  $\triangleright$  sparse NNLS solver
7:    $\boldsymbol{\mu} \leftarrow \mathbf{G}^T(\mathbf{b} - \mathbf{G}\boldsymbol{\xi})$ 
8:    $[\nu, e] \leftarrow \text{max}(\boldsymbol{\mu})$   $\triangleright$  max: returns maximum value in a vector followed by its location (index)
9:    $E \leftarrow E \cup \{e\}, Z \leftarrow Z \setminus \{e\}$ 
10:  while true do
11:     $\zeta_E \leftarrow \mathbf{G}_E^\dagger \mathbf{b}$   $\triangleright \dagger$  represents pseudo-inverse
12:     $\zeta_Z \leftarrow \mathbf{0}$ 
13:    if  $\zeta_E > \mathbf{0}$  then
14:       $\boldsymbol{\xi} \leftarrow \zeta$ 
15:      break
16:    end if
17:     $\eta \leftarrow \min_{k \in E} \xi_k / (\xi_k - \zeta_k)$ 
18:     $\boldsymbol{\xi} \leftarrow \boldsymbol{\xi} + \eta(\zeta - \boldsymbol{\xi})$ 
19:     $Z \leftarrow \{i | \xi_i = 0\}$ 
20:     $E \leftarrow \{1, \dots, n_e\} \setminus Z$ 
21:  end while
22: end while
```

3.2 Preservation of Lagrangian structure and numerical stability

3.2.1 Conservative systems

Following similar steps as in [7], we show here that the hyper-reduced model preserves the Lagrangian structure, leading to numerical stability of the hyper-reduced model. For this purpose, we restrict our discussion to a conservative system, where the Hamiltonian principle represents the conservation of total mechanical energy as follows:

$$\mathcal{E} = \mathcal{T}(\dot{\mathbf{u}}) + \mathcal{V}(\mathbf{u}) = \text{constant}, \quad (15)$$

where \mathcal{T} and \mathcal{V} are the functionals associated to the kinetic energy and the potential energy of the system, respectively. The kinetic energy is given by

$$\mathcal{T}(\dot{\mathbf{u}}) = \frac{1}{2} \dot{\mathbf{u}}^T \mathbf{M} \dot{\mathbf{u}} = \sum_{e=1}^{n_e} \underbrace{\frac{1}{2} \dot{\mathbf{u}}_e^T \mathbf{M}_e \dot{\mathbf{u}}_e}_{\mathcal{T}_e(\mathbf{u}_e)}, \quad (16)$$

where $\mathbf{M}_e \in \mathbb{R}^{N_e \times N_e}$ is the contribution of the element e towards the mass matrix. Furthermore, the potential energy can be written as

$$\mathcal{V}(\mathbf{u}) = - \underbrace{\int \mathbf{f}(\mathbf{u}) \cdot d\mathbf{u}}_{\mathcal{V}^{int}(\mathbf{u})} + \underbrace{\int \mathbf{g} \cdot d\mathbf{u}}_{\mathcal{V}^{ext}(\mathbf{u})}, \quad (17)$$

such that

$$\mathbf{f}(\mathbf{u}) = -\frac{\partial \mathcal{V}^{int}(\mathbf{u})}{\partial \mathbf{u}}, \quad (18)$$

$$\mathbf{g}(\mathbf{u}) = -\frac{\partial \mathcal{V}^{ext}(\mathbf{u})}{\partial \mathbf{u}}, \quad (19)$$

and \mathcal{V}^{int} and \mathcal{V}^{ext} are the potential energies associated to internal and external forces, respectively. The conservative counterpart of the equations of motion (1) can then be expressed using Lagrange equations as:

$$\frac{d}{dt} \left(\frac{\partial \mathcal{T}(\dot{\mathbf{u}})}{\partial \dot{\mathbf{u}}} \right) + \frac{\partial \mathcal{V}^{int}(\mathbf{u})}{\partial \mathbf{u}} = \mathbf{g}. \quad (20)$$

As shown in , the reduced-order model, obtained by introduction of a nonlinear mapping $\mathbf{\Gamma}$ and projection of the resulting equations to the tangent space $\mathbf{P}_{\mathbf{\Gamma}}$ of the manifold, is given by

$$\mathbf{P}_{\mathbf{\Gamma}}^T \left[\frac{d}{dt} \left(\frac{\partial \mathcal{T}(\dot{\mathbf{\Gamma}}(\mathbf{q}))}{\partial \dot{\mathbf{\Gamma}}(\mathbf{q})} \right) + \frac{\partial \mathcal{V}^{int}(\mathbf{\Gamma}(\mathbf{q}))}{\partial \mathbf{\Gamma}(\mathbf{q})} \right] = \mathbf{P}_{\mathbf{\Gamma}}^T \mathbf{g}, \quad (21)$$

where $\mathbf{\Gamma} : \mathbb{R}^n \mapsto \mathbb{R}^m$ describes a general nonlinear mapping which approximates the solution \mathbf{u} using a reduced set of unknowns \mathbf{q} . It is easy to see that this equation is equivalent to ROM (3) in the conservative setting, i.e.,

$$\mathbf{P}_{\mathbf{\Gamma}}^T \left[\mathbf{M} \ddot{\mathbf{\Gamma}}(\mathbf{q}) + \frac{\partial \mathcal{V}^{int}(\mathbf{\Gamma}(\mathbf{q}))}{\partial \mathbf{\Gamma}(\mathbf{q})} \right] = \mathbf{P}_{\mathbf{\Gamma}}^T \mathbf{g} \quad (22)$$

As is shown below, the projection of the equations to the tangent space of the manifold is essential for preserving the Lagrangian structure associated to the corresponding Hamiltonian principle. Note that ROM obtained using a Galerkin projection is a special case of the general setting in (22) when a linear mapping $\mathbf{\Gamma}(\mathbf{q}) = \mathbf{V}\mathbf{q}$ is used. It is well known (as also shown in [7]) that such a Galerkin projection is structure-preserving. We show here that this is also true for ROM (22), obtained by projection on to the tangent space of general nonlinear manifolds.

The Hamiltonian, associated to (22), is given by

$$\begin{aligned} \mathcal{E}_r(\mathbf{q}, \dot{\mathbf{q}}) &= \mathcal{T}(\dot{\mathbf{\Gamma}}(\mathbf{q})) + \mathcal{V}(\mathbf{\Gamma}(\mathbf{q})), \\ \implies \dot{\mathcal{E}}_r(\mathbf{q}, \dot{\mathbf{q}}, \ddot{\mathbf{q}}) &= \dot{\mathcal{T}}(\dot{\mathbf{\Gamma}}(\mathbf{q})) + \dot{\mathcal{V}}(\mathbf{\Gamma}(\mathbf{q})) \\ &= \frac{\partial \mathcal{T}(\dot{\mathbf{\Gamma}}(\mathbf{q}))}{\partial \dot{\mathbf{\Gamma}}(\mathbf{q})} \ddot{\mathbf{\Gamma}}(\mathbf{q}) + \frac{\partial \mathcal{V}^{int}(\mathbf{\Gamma}(\mathbf{q}))}{\partial \mathbf{\Gamma}(\mathbf{q})} \dot{\mathbf{\Gamma}}(\mathbf{q}) - \frac{\partial \mathcal{V}^{ext}(\mathbf{\Gamma}(\mathbf{q}))}{\partial \mathbf{\Gamma}(\mathbf{q})} \dot{\mathbf{\Gamma}}(\mathbf{q}) \\ &= (\dot{\mathbf{\Gamma}}(\mathbf{q}))^T \mathbf{M} \ddot{\mathbf{\Gamma}}(\mathbf{q}) + (\dot{\mathbf{\Gamma}}(\mathbf{q}))^T \frac{\partial \mathcal{V}^{int}(\mathbf{\Gamma}(\mathbf{q}))}{\partial \mathbf{\Gamma}(\mathbf{q})} - (\dot{\mathbf{\Gamma}}(\mathbf{q}))^T \mathbf{g} \\ &= \dot{\mathbf{q}}^T \left(\mathbf{P}_{\mathbf{\Gamma}}^T \left[\mathbf{M} \ddot{\mathbf{\Gamma}}(\mathbf{q}) + \frac{\partial \mathcal{V}^{int}(\mathbf{\Gamma}(\mathbf{q}))}{\partial \mathbf{\Gamma}(\mathbf{q})} - \mathbf{g} \right] \right) \quad (\because \dot{\mathbf{\Gamma}}(\mathbf{q}) = \mathbf{P}_{\mathbf{\Gamma}} \dot{\mathbf{q}}) \\ &= 0 \quad (\text{Using (22)}) \end{aligned} \quad (23)$$

Thus, $\mathcal{E}_r = \text{constant}$, and the total mechanical energy is conserved for ROM in (22).

Having established that tangent space projection leads to structure-preserving ROMs, we now show that the same is true for hyper-reduced model obtained using EECSW, where the reduced internal force from (22) is approximated (cf. (8)) as follows:

$$\hat{\mathbf{f}}(\mathbf{q}) = \mathbf{P}_{\mathbf{\Gamma}}^T \mathbf{f}(\mathbf{\Gamma}(\mathbf{q})) = \mathbf{P}_{\mathbf{\Gamma}}^T \frac{\partial \mathcal{V}^{int}(\mathbf{\Gamma}(\mathbf{q}))}{\partial \mathbf{\Gamma}(\mathbf{q})} = \sum_{e=1}^{n_e} (\mathbf{P}_{\mathbf{\Gamma}}^T)_e \frac{\partial \mathcal{V}_e^{int}(\mathbf{\Gamma}_e(\mathbf{q}))}{\partial \mathbf{\Gamma}_e(\mathbf{q})} \approx \sum_{e \in E} \xi_e (\mathbf{P}_{\mathbf{\Gamma}}^T)_e \frac{\partial \mathcal{V}_e^{int}(\mathbf{\Gamma}_e(\mathbf{q}))}{\partial \mathbf{\Gamma}_e(\mathbf{q})}. \quad (24)$$

Furthermore, the inertial force can also be approximated as

$$\mathbf{P}_\Gamma^T \mathbf{M} \ddot{\Gamma}(\mathbf{u}) = \sum_{e=1}^{n_e} (\mathbf{P}_\Gamma^T)_e \mathbf{M}_e \ddot{\Gamma}_e(\mathbf{q}) \approx \sum_{e \in E} \xi_e (\mathbf{P}_\Gamma^T)_e \mathbf{M}_e \ddot{\Gamma}_e(\mathbf{q}) = \sum_{e \in E} \xi_e (\mathbf{P}_\Gamma^T)_e \frac{d}{dt} \frac{\partial \mathcal{T}_e(\dot{\Gamma}_e(\mathbf{q}))}{\partial \dot{\Gamma}_e(\mathbf{q})}. \quad (25)$$

Thus, it follows from (24) that the potential energy $\mathcal{V}^{int}(\Gamma(\mathbf{q}))$ associated to the reduced internal force can also be approximated as

$$\mathcal{V}_r^{int}(\mathbf{q}) := \mathcal{V}^{int}(\Gamma(\mathbf{q})) \approx \tilde{\mathcal{V}}_r^{int}(\mathbf{q}) = \sum_{e \in E} \xi_e \mathcal{V}_e^{int}(\Gamma_e(\mathbf{q})), \quad (26)$$

and from (25) that the kinetic energy, $\mathcal{T}(\dot{\Gamma}(\mathbf{q}))$, can be approximated as

$$\mathcal{T}_r(\dot{\mathbf{q}}, \mathbf{q}) := \mathcal{T}(\dot{\Gamma}(\mathbf{q})) \approx \tilde{\mathcal{T}}_r(\dot{\mathbf{q}}, \mathbf{q}) = \sum_{e \in E} \xi_e \mathcal{T}_e(\dot{\Gamma}_e(\mathbf{q})), \quad (27)$$

Here, $\tilde{\mathcal{V}}_r^{int}(\mathbf{q})$ and $\tilde{\mathcal{T}}_r(\dot{\mathbf{q}}, \mathbf{q})$ are the potential and the kinetic energy associated to the hyper-reduced system of equations given as:

$$\sum_{e \in E} \xi_e (\mathbf{P}_\Gamma^T)_e \mathbf{M}_e \ddot{\Gamma}_e(\mathbf{q}) + \sum_{e \in E} \xi_e (\mathbf{P}_\Gamma^T)_e \frac{\partial \mathcal{V}_e^{int}(\Gamma_e(\mathbf{q}))}{\partial \Gamma_e(\mathbf{q})} = \mathbf{P}_\Gamma^T \mathbf{g}. \quad (28)$$

Analogous to the previous discussion, the Hamiltonian associated to the hyper-reduced system becomes

$$\begin{aligned} \tilde{\mathcal{E}}_r(\mathbf{q}, \dot{\mathbf{q}}) &= \tilde{\mathcal{T}}_r(\dot{\mathbf{q}}, \mathbf{q}) + \tilde{\mathcal{V}}_r^{int}(\mathbf{q}) + \mathcal{V}^{ext}(\Gamma(\mathbf{q})) \\ \implies \dot{\tilde{\mathcal{E}}}_r(\mathbf{q}, \dot{\mathbf{q}}, \ddot{\mathbf{q}}) &= \dot{\tilde{\mathcal{T}}}_r(\dot{\mathbf{q}}, \mathbf{q}) + \dot{\tilde{\mathcal{V}}}_r^{int}(\mathbf{q}) + \dot{\mathcal{V}}^{ext}(\Gamma(\mathbf{q})) \\ &= \dot{\mathbf{q}}^T \left(\sum_{e \in E} \xi_e (\mathbf{P}_\Gamma^T)_e \mathbf{M}_e \ddot{\Gamma}_e(\mathbf{q}) + \sum_{e \in E} \xi_e (\mathbf{P}_\Gamma^T)_e \frac{\partial \mathcal{V}_e^{int}(\Gamma_e(\mathbf{q}))}{\partial \Gamma_e(\mathbf{q})} - \mathbf{P}_\Gamma^T \mathbf{g} \right) \\ &= 0 \quad (\text{Using (28)}). \end{aligned}$$

This shows that EECSW for ROMs given by (3) preserves the Lagrangian structure and conserves energy according to the Hamilton's principle for a conservative mechanical system. The numerical stability of the hyper-reduced model is a direct consequence of this structure-preserving property as noted in [7], as well.

3.2.2 Dissipative, non-conservative systems

To include dissipation effects which, typically, generate forces opposite to the generalized velocity vector $\dot{\mathbf{u}}$ in the system, a dissipation functional \mathcal{D} can be defined, such that the corresponding forces are given by

$$\mathbf{f}^{dis}(\dot{\mathbf{u}}) = - \frac{\partial \mathcal{D}(\dot{\mathbf{u}})}{\partial \dot{\mathbf{u}}}.$$

Assuming that the functional \mathcal{D} has the same degree of homogeneity, m , in the generalized velocities ($\dot{\mathbf{u}}$) for all elements in the mesh, we have

$$\dot{\mathbf{u}}^T \frac{\partial \mathcal{D}(\dot{\mathbf{u}})}{\partial \dot{\mathbf{u}}} = \sum_{e=1}^{n_e} \dot{\mathbf{u}}_e^T \frac{\partial \mathcal{D}_e(\dot{\mathbf{u}}_e)}{\partial \dot{\mathbf{u}}_e} = m \sum_{e=1}^{n_e} \mathcal{D}_e(\dot{\mathbf{u}}_e), \quad (29)$$

where \mathcal{D}_e is the usual notation for the contribution of element e towards the total dissipation \mathcal{D} , which would be dependent on the nodal velocities $\dot{\mathbf{u}}_e$ only. For the special case of viscous damping, i.e., $m = 2$, we have

$$\mathcal{D}(\dot{\mathbf{u}}) = \frac{1}{2} \dot{\mathbf{u}}^T \mathbf{C} \dot{\mathbf{u}}.$$

Other values of m lead to different types of dissipation models, e.g., $m = 1$ leads to dry Coloumb friction and $m = 3$ leads to a viscous drag in fluids.

The Hamilton's principle in this non-conservative setting leads to

$$\dot{\mathcal{T}} + \dot{\mathcal{V}} = \left(-\frac{\partial \mathcal{D}(\dot{\mathbf{u}})}{\partial \dot{\mathbf{u}}} + \mathbf{f}^{nc} \right) \cdot \dot{\mathbf{u}} = \dot{\mathbf{u}}^T \mathbf{f}^{nc} - m \sum_{e=1}^{n_e} \mathcal{D}_e(\dot{\mathbf{u}}_e), \quad (30)$$

where \mathbf{f}^{nc} is a non-conservative, time-dependent external force. The corresponding Lagrange equations of motion can then be expressed, equivalently, as

$$\mathbf{M}\ddot{\mathbf{u}} + \frac{\partial \mathcal{D}(\dot{\mathbf{u}})}{\partial \dot{\mathbf{u}}} + \frac{\partial \mathcal{V}^{int}(\mathbf{u})}{\partial \mathbf{u}} = \mathbf{g} + \mathbf{f}^{nc}. \quad (31)$$

Following the same procedure as shown above for conservative systems, it is easy to show that the Lagrangian structure is preserved using EECSW for non-conservative systems, as well.

The nonlinear ROM associated to (31) is given by

$$\mathbf{P}_\Gamma^T \left[\mathbf{M}\ddot{\Gamma}(\mathbf{q}) + \frac{\partial \mathcal{D}(\dot{\Gamma}(\mathbf{q}))}{\partial \dot{\Gamma}(\mathbf{q})} + \frac{\partial \mathcal{V}^{int}(\Gamma(\mathbf{q}))}{\partial \Gamma(\mathbf{q})} \right] = \mathbf{P}_\Gamma^T [\mathbf{g} + \mathbf{f}^{nc}], \quad (32)$$

The approximation of the additional nonlinear term in (32) using EECSW is given by

$$\mathbf{P}_\Gamma^T \frac{\partial \mathcal{D}(\dot{\Gamma}(\mathbf{q}))}{\partial \dot{\Gamma}(\mathbf{q})} = \sum_{e=1}^{n_e} (\mathbf{P}_\Gamma^T)_e \frac{\partial \mathcal{D}_e(\dot{\Gamma}_e(\mathbf{q}))}{\partial \dot{\Gamma}_e(\mathbf{q})} \approx \sum_{e \in E} (\mathbf{P}_\Gamma^T)_e \frac{\partial \mathcal{D}_e(\dot{\Gamma}_e(\mathbf{q}))}{\partial \dot{\Gamma}_e(\mathbf{q})}. \quad (33)$$

It follows that the dissipation can be approximated as

$$\mathcal{D}_r(\dot{\mathbf{q}}, \mathbf{q}) := \mathcal{D}(\dot{\Gamma}(\mathbf{q})) \approx \tilde{\mathcal{D}}_r(\dot{\mathbf{q}}, \mathbf{q}) = \sum_{e \in E} \xi_e \mathcal{D}_e(\dot{\Gamma}_e(\mathbf{q})), \quad (34)$$

where $\tilde{\mathcal{D}}_r$ can be thought of as the dissipation associated to the hyper-reduced model given by

$$\sum_{e \in E} \xi_e (\mathbf{P}_\Gamma^T)_e \left[\mathbf{M}_e \ddot{\Gamma}_e(\mathbf{q}) + \frac{\partial \mathcal{D}_e(\dot{\Gamma}_e(\mathbf{q}))}{\partial \dot{\Gamma}_e(\mathbf{q})} + \frac{\partial \mathcal{V}_e^{int}(\Gamma_e(\mathbf{q}))}{\partial \Gamma_e(\mathbf{q})} \right] = \mathbf{P}_\Gamma^T [\mathbf{g} + \mathbf{f}^{nc}]. \quad (35)$$

The rate of change of the total energy $\tilde{\mathcal{E}}_r$ associated to the hyper-reduced model (35) is given by

$$\begin{aligned} \dot{\tilde{\mathcal{E}}}_r(\mathbf{q}, \dot{\mathbf{q}}, \ddot{\mathbf{q}}) &= \dot{\tilde{T}}_r(\dot{\mathbf{q}}, \mathbf{q}) + \dot{\mathcal{V}}_r^{int}(\mathbf{q}) + \dot{\mathcal{V}}^{ext}(\Gamma(\mathbf{q})) - \frac{d}{dt} (\Gamma(\mathbf{q}) \cdot \mathbf{f}^{nc}) \\ &= \dot{\mathbf{q}}^T \left(\sum_{e \in E} \xi_e (\mathbf{P}_\Gamma^T)_e \left[\mathbf{M}_e \ddot{\Gamma}_e(\mathbf{q}) + \frac{\partial \mathcal{V}_e^{int}(\Gamma_e(\mathbf{q}))}{\partial \Gamma_e(\mathbf{q})} \right] - \mathbf{P}_\Gamma^T [\mathbf{g} + \mathbf{f}^{nc}] \right) - \Gamma(\mathbf{q}) \cdot \dot{\mathbf{f}}^{nc} \\ &= - \sum_{e \in E} \xi_e \dot{\mathbf{q}}^T (\mathbf{P}_\Gamma^T)_e \frac{\partial \mathcal{D}_e(\dot{\Gamma}_e(\mathbf{q}))}{\partial \dot{\Gamma}_e(\mathbf{q})} - \Gamma(\mathbf{q}) \cdot \dot{\mathbf{f}}^{nc} \quad (\text{Using (35)}) \\ &= - \sum_{e \in E} \xi_e (\dot{\Gamma}_e(\mathbf{q}))^T \frac{\partial \mathcal{D}_e(\dot{\Gamma}_e(\mathbf{q}))}{\partial \dot{\Gamma}_e(\mathbf{q})} - \Gamma(\mathbf{q}) \cdot \dot{\mathbf{f}}^{nc} \\ &= -m \tilde{\mathcal{D}}_r(\dot{\mathbf{q}}, \mathbf{q}) - \Gamma(\mathbf{q}) \cdot \dot{\mathbf{f}}^{nc} \quad (\text{Using (29), (34)}) \\ &\implies \dot{\tilde{T}}_r(\dot{\mathbf{q}}, \mathbf{q}) + \dot{\mathcal{V}}_r^{int}(\mathbf{q}) + \dot{\mathcal{V}}^{ext}(\Gamma(\mathbf{q})) = -m \tilde{\mathcal{D}}_r(\dot{\mathbf{q}}, \mathbf{q}) + (\dot{\Gamma}(\mathbf{q}))^T \mathbf{f}^{nc}. \quad (36) \end{aligned}$$

When compared with (30) and (34), Equation (36) proves that EECSW preserves the Lagrangian structure associated to the Hamiltonian principle for a non-conservative system, as well.

The conditional/unconditional numerical stability properties of any chosen time integration scheme are carried over to the hyper-reduced model as a direct consequence of the energy-conserving/structure-preserving properties of EECSW. We refer the reader to Section 4.3 in [7] for the discussion on how these properties lead to numerical stability.

4 Numerical results

4.1 Setup

To test and illustrate the performance of the EECSW method, proposed here, we require a high-dimensional system which can be reduced using a suitable nonlinear mapping. To this end, we use the quadratic manifold, introduced in [11], for model reduction. In the quadratic manifold approach, the full set of unknowns \mathbf{u} are mapped to a lower dimensional set of variables \mathbf{q} using a quadratic mapping as

$$\mathbf{u} \approx \mathbf{\Gamma}(\mathbf{q}) := \mathbf{\Phi}\mathbf{q} + \frac{1}{2}\mathbf{\Omega} : (\mathbf{q} \otimes \mathbf{q}), \quad (37)$$

where the columns of $\mathbf{\Phi} \in \mathbb{R}^{n \times M}$ contains M significant vibration modes (VMs) extracted at equilibrium $\mathbf{u} = \mathbf{0}$, and $\mathbf{\Omega} \in \mathbb{R}^{n \times M \times M}$ is a third-order tensor containing the corresponding static modal derivatives (SMDs). The symbol \otimes denotes the dyadic product, while $:$ indicates contraction over the last two indexes.²

For consistency, we use the same examples used in [11]: Model-I, a flat plate, simply-supported on two opposite sides, and Model-II, a NACA-airfoil-based wing model. The details of both models are shown in Figures 1 and 3. Time integration is performed using the implicit Newmark scheme with a time step constant across all techniques for a fair comparison. Both structures are discretized using flat, triangular-shell elements with 6 DOFs per node, i.e., 18 DOFs per element. For both models, the accuracy of the results is compared to the corresponding full nonlinear solutions using a mass-normalized global relative error (GRE) measure, defined as

$$GRE_M = \frac{\sqrt{\sum_{t \in S} (\mathbf{u}(t) - \tilde{\mathbf{u}}(t))^T \mathbf{M} (\mathbf{u}(t) - \tilde{\mathbf{u}}(t))}}{\sqrt{\sum_{t \in S} \mathbf{u}(t)^T \mathbf{M} \mathbf{u}(t)}} \times 100,$$

where $\mathbf{u}(t) \in \mathbb{R}^n$ is the vector of generalized displacements at the time t , obtained from the HFM solution, $\tilde{\mathbf{u}}(t) \in \mathbb{R}^n$ is the solution based on the (hyper)reduced model, and S is the set of time instants at which the error is recorded. The mass matrix \mathbf{M} provides a relevant normalization for the generalized displacements, which could be a combination of physical displacements and rotations, as is the case in the shell models shown here.

The computations were performed on the Euler cluster of ETH Zürich. Since the success of reduction techniques is often reported in terms of savings in simulation time, we define an online speedup S^* computed according to the following simple formula:

$$S^* = \frac{T_{full}}{T_{sim}^*},$$

where T_{full} and T_{sim}^* represent the CPU time taken during the time integration of *full* and (hyper)reduced solution respectively. The superscript \star denotes the reduction technique being used.

²The mapping (37) can be written using the Einstein summation convention in the indicial notation as: $\Gamma_I = \Phi_{Ii}q_j + \frac{1}{2}\Omega_{Iij}q_iq_j$ $I \in \{1, \dots, n\}$, $i, j \in \{1, \dots, M\}$

We compare the hyper-reduction using ECSW (where the ROMs are obtained from linear mappings), with the EECSW method. For both ECSW and EECSW, the convergence tolerance τ for finding a sparse solution to the NNLS problem (14), as required in Algorithm 1, is chosen to be 0.01. This is within the practically recommended range as reported in [5]. A total of $n_t = 200$ training vectors, chosen uniformly from the solution time-span, are used in sparse NNLS routine. The following ROMs are considered in our comparison:

- *Linear-mapping-based (Hyper-)Reduction:*

POD: Here, the first most significant m Proper Orthogonal Decomposition (POD) modes obtained from the HFM run are used to construct \mathbf{V} . For a fair comparison, m is taken equal as in **LM**.

ECSW-POD: Hyper-reduction using ECSW is performed, for the ROM obtained in the POD approach. This is the original ECSW implementation as proposed in [5].

- *Quadratic-manifold-based (Hyper-)Reduction:*

QM: Here, the quadratic mapping (37) is used to construct the ROM as given by (3).

EECSW-QM: The ROM obtained in QM approach using the quadratic manifold is hyper-reduced using the EECSW.

4.2 Flat Structure

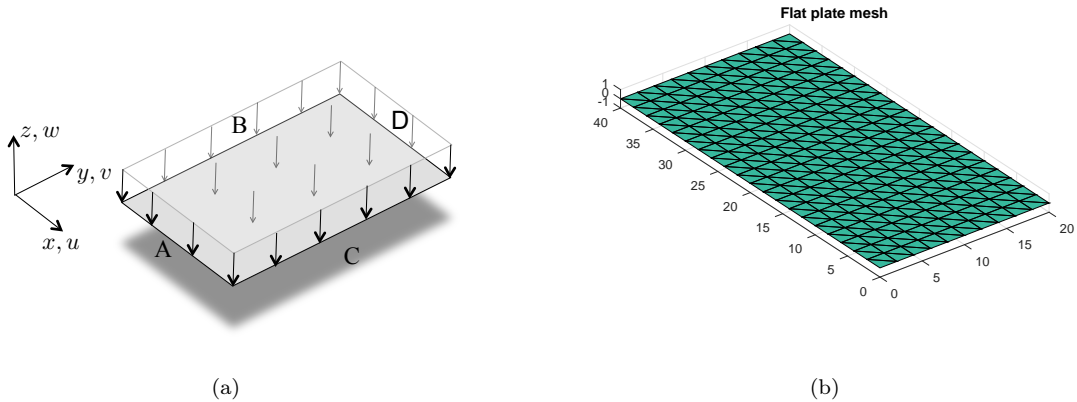
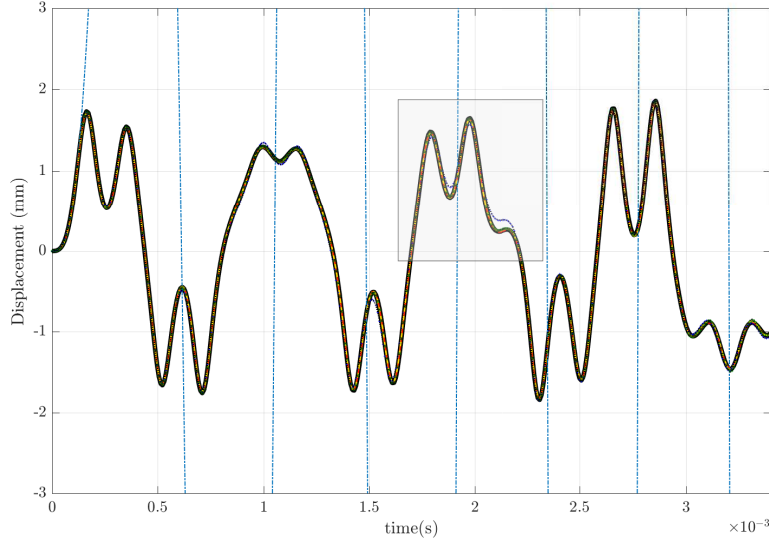


Figure 1: **Model - I:** (a) Flat plate example - simply supported on sides A and D . The plate is $L = 40$ mm long, $H = 20$ mm wide, $t = 0.8$ mm thick. The Young Modulus is $E = 70$ GPa, the Poisson's ratio is $\nu = 0.33$, and the density is $\rho = 2700$ Kg/m³. A uniform pressure is applied on the plate, according to the time history $p(t) = P \sin(\omega t)$, where $P = 1$ N/mm² and $\omega = 2.097 \times 10^4$ rad/s. (b) The curved plate is discretized using flat, triangular shell elements. The FE mesh contains 400 elements and 1386 DOFs. The two opposite sides parallel to the y -axis are simply supported, a uniform pressure is applied on the curved surface, according to the time history.

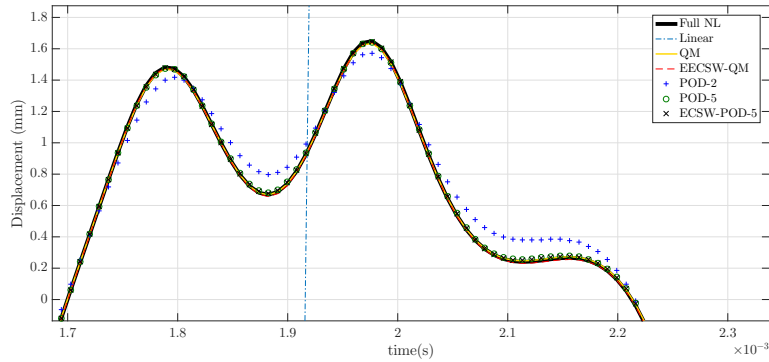
We consider the rectangular flat plate structure shown in Figure 1. A uniform pressure distribution is chosen to act normal to the plate surface as the external load. A time varying amplitude (load function) is used given by

$$\begin{aligned} \mathbf{g}(t) &= p(t)\mathbf{1}, \\ p(t) &= \sin(\omega t), \end{aligned} \tag{38}$$

where \mathbf{l} is a constant load vector corresponding to a uniform pressure distribution of 1 N/mm^2 . Here, $p(t)$, termed as the dynamic load function, determines the time-dependency of the external load. The results are shown for a periodic choice for $p(t)$ as given by (38), where ω is chosen to be the first natural frequency of the linearized system. Due to the resonant nature of the dynamic, it is easy to excite geometrically nonlinear behavior in the system, as shown by Figure 2. Furthermore, Figure 2 shows that the full nonlinear solution is reduced using the QM technique and, subsequently, hyper-reduced using EECSW with good accuracy.



(a)



(b)

Figure 2: The linear solution (dashed-blue) grows quickly to high amplitudes for the choice of resonant loading; the full solution (thick black) shows much lower amplitudes due to the geometrical nonlinearities; the ROM obtained using quadratic manifold (yellow) and hyper-reduced solution for this ROM using EECSW (dashed-red) capture the full solution accurately. Subfigure (b) highlights the inaccuracy of the POD ROM with $m = 2$.

It can also be confirmed from the global relative error GRE_M and speed-up S^* , shown in Table 1, that the QM based nonlinear ROM reproduces the results of Model-I with good accuracy but, as expected, does not deliver a good speed-up. The EECSW-based hyper-reduction, on the other hand, gives results with a GRE_M of 1.37% but delivers a much higher speed-up of about 100. Note

also that a linear-mapping-based ROM with POD of the same size ($m = 2$) as the adopted nonlinear mapping does not deliver a good accuracy.

Reduction Technique	Basis size (m)	# elements	$GRE_M(\%)$	S^*
POD	2	400	5.62	2.96
POD	5	400	1.81	2.84
ECSW-POD	5	12	2.52	77.7
QM	2	400	1.32	3.03
EECSW-QM	2	6	1.37	99.93

Table 1: Comparison of global relative error GRE_M and speed-ups in Model-I for linear-mapping-based ROMs and their hyper-reduced counterparts on one hand, and for quadratic-manifold-based ROMs and their hyper-reduced counterparts using EECSW on the other hand. Time for a full solution run $T_{full} = 74.4$ s.

4.3 Wing Structure

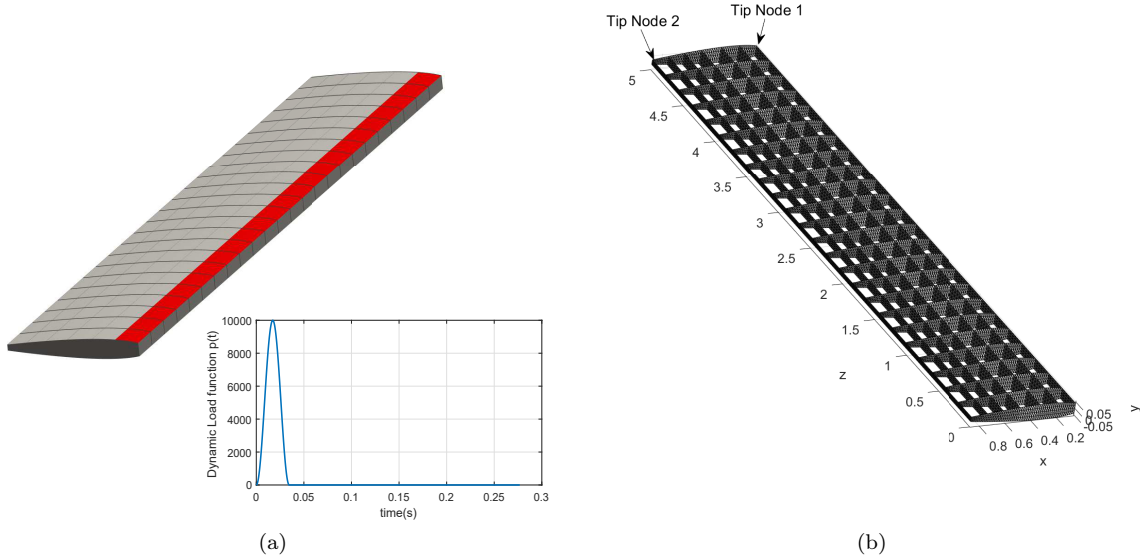


Figure 3: **Model - II:** (a) A wing structure with NACA 0012 airfoil (length(L) = 5 m, Width(W) \approx 0.9 m, Height(H) = 0.1 m) stiffened with ribs along the longitudinal and lateral direction. The Young Modulus is $E = 70$ GPa, the Poisson's ratio is $\nu = 0.33$, and the density is $\rho = 2700$ Kg/m³. The wing is cantilevered at one end. Uniform pressure is applied on the highlighted area, with a pulse load as given by (39); (b) The structure is meshed with triangular flat shell elements with 6 DOFs per node and each with a thickness of 1.5 mm. The mesh contains $n = 135770$ DOFs, $n_e = 49968$ elements. For illustration purposes, the skin panels are removed, and mesh is shown.

For the application of the proposed simulation-free hyper-reduction methods to more realistic models, we consider the model of a NACA-airfoil-based wing structure, introduced in [11]. This model, referred to as Model-II, contains truly high number of DOFs ($n = 135770$), thereby, allowing for the appreciation of obtained accuracy and computational speed-ups. We simulate the response of

the structure to a low frequency pulse load, applied as a spatially uniform pressure load on the highlighted area on the structure skin (cf. Figure 3). The dynamic load function, shown in Figure 4a, is given as

$$p(t) = A \sin^2(\omega t) \left[H(t) - H\left(\frac{\pi}{\omega} - t\right) \right], \quad (39)$$

where $H(t)$ is the Heaviside function and ω chosen as the mean of the first and second natural frequency of vibration. We refer the reader to [11] for the detailed linearized, full nonlinear and reduced nonlinear response plots of this model.

Figure 4b and Table 2 show that the hyper-reduction using EECSW for the quadratic-manifold based ROM reproduce the full system response with a very good accuracy ($GRE_M \approx 1.71\%$) and is more than a thousand times faster than the full response computation. As expected, we obtain a much higher speed-up during hyper-reduction in comparison with Model-I. The speed-up without hyper-reduction, however, are fairly similar between the two models, despite the striking difference in the number of DOFs. Thus, the numerical results confirm the need and effectiveness of EECSW for hyper-reduction of large nonlinear systems over nonlinear manifolds.

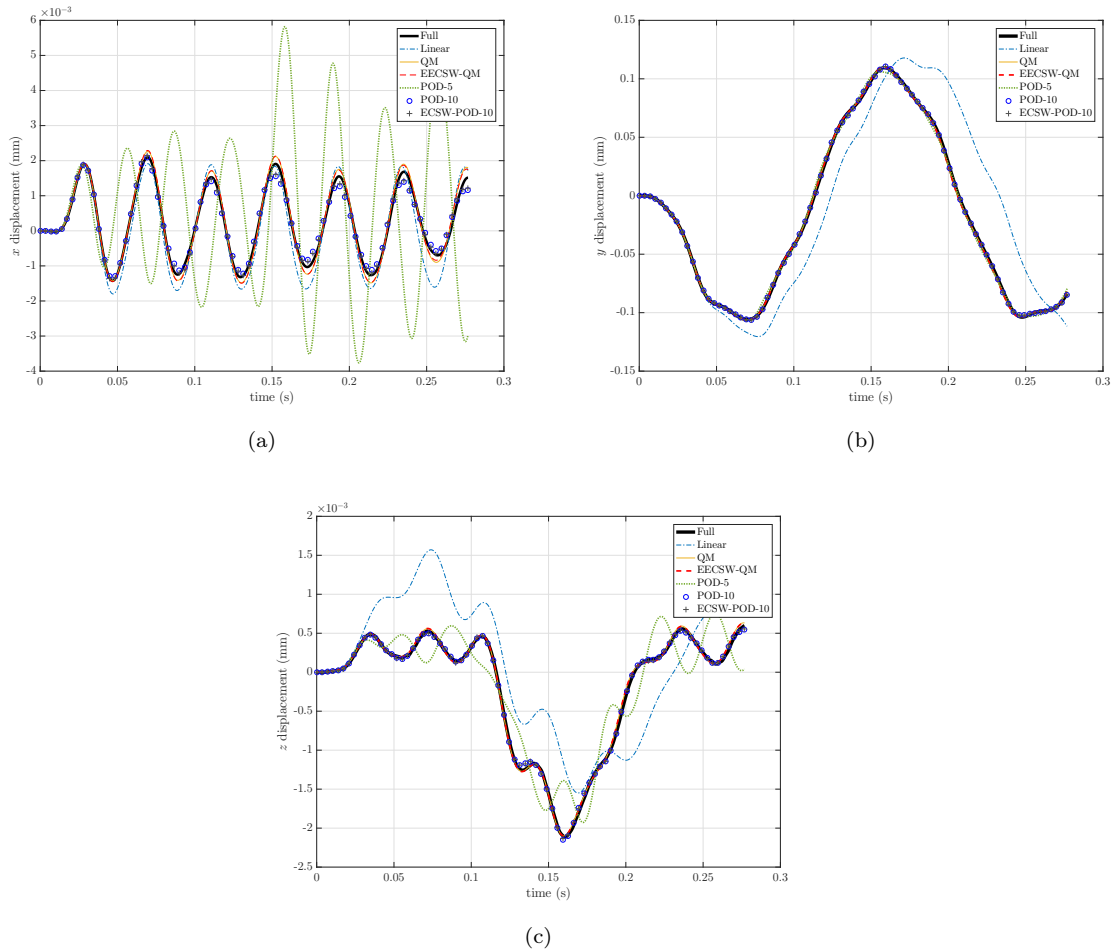


Figure 4: (a), (b), (c): Comparison of full, linear and various reduced responses at tip node 2 in x , y and z directions. Note that the QM-based reduced solution (with 5 reduced unknowns) accurately captures the full system response, whereas the POD-based ROM with 5 modes fails to reproduce the nonlinear system response (POD-5).

Figure 4 and Table 2 compare the response of Model-II to the applied load. Figure 4 further shows that the response of the full system is captured more effectively using the quadratic manifold as compared to the POD with the same number of unknowns (POD-5). This underscores the importance of nonlinear manifolds in model reduction of nonlinear systems. In terms of speed as well, we see in Table 2 that the EECSW method performs better than its linear counterpart.

Reduction Technique	Basis size (m)	# elements	$GRE_M(\%)$	S^*
POD	5	49968	5.01	3.07
POD	10	49968	0.98	2.77
ECSW-POD	10	152	1.05	794.6
QM	5	49968	1.65	2.92
EECSW-QM	5	44	1.71	1098

Table 2: Starting with a linear modal superposition with $M = 5$ modes (first 5 VMs), reduction techniques as described in Section 4.1 are formulated. Global Relative Error and speed-ups in Model-II for these reduction techniques are tabulated. A total of $n_t = 200$ training vectors, chosen uniformly from the solution time-span, are used to setup hyper-reduction in ECSW-POD and EECSW-QM. Time for a full solution run $T_{full} = 3.808 \times 10^4$ s.

It is interesting to see that EECSW-QM ends up sampling a much smaller set of elements as compared to its linear counterpart EECSW-POD. The corresponding speed-up for EECSW-QM, however, doesn't show a proportionate increase. This can be explained on two accounts:

1. The additional convective terms in the nonlinear-mapping-based ROM (4) adds to the computational burden in comparison with its linear counterpart (5)
2. The evaluation of the nonlinear mapping (quadratic in this case), is expected to be more expensive than a linear mapping, which boils down to a standard matrix-vector product. Though MATLAB is extremely efficient at performing such matrix-vector products, and hence, in the evaluation of linear mappings, the same cannot be said about our sub-optimal implementation for evaluation of the quadratic mapping at hand.

Nonetheless, in our numerical tests, EECSW more than compensates for these extra costs by outperforming ECSW-POD in terms of speed.

5 Conclusion

We have extended the concept of hyper-reduction for model reduction over nonlinear manifolds of nonlinear, FE-based mechanical systems. In particular, the recently developed ECSW technique has been extended to allow for hyper-reduction using smooth nonlinear mappings into the reduced system of unknowns. In doing so, we showed that the ROM obtained by projection onto the tangent space of the manifold, leads to the preservation of structure and stability properties of the ECSW method.

We demonstrated the EECSW method on two structural dynamics examples by hyper-reduction of a ROM based on the quadratic manifold, whereby better speed and accuracy were obtained using the EECSW method in comparison with ECSW-POD based hyper-reduced models. Since these models were based on von-Karman nonlinearities, the degree of nonlinearity in the examples is expected to be much lower than the nominal thin-walled structures featuring geometrically nonlinear behavior. A quadratic manifold was, therefore, effective in capturing the nonlinear behavior effectively for these structures. However, nonlinear manifolds – possibly constructed from solution databases – would play a crucial role in the effective reduction of models with higher degree of nonlinearities.

EECSW in such cases is expected to play a vital role during the hyper-reduction stage by providing the necessary computational speed-ups. Testing the EECSW on ROMs based on nonlinear manifolds constructed using data-driven techniques would be a part of our future endeavours.

Acknowledgements The authors acknowledge the support of the Air Force Office of Scientific Research, Air Force Material Command, USAF under Award No.FA9550-16-1-0096. We also thank Ludovic Renson for pointing us to the MATLAB-based tensor product toolbox TPROD.

References

- [1] Chaturantabut, S., Sorensen, D. C. Nonlinear model reduction via discrete empirical interpolation, *SIAM Journal on Scientific Computing* (2010) 32(5): 2737-2764. DOI: 10.1137/090766498
- [2] Tiso, P., Rixen, D. J. (2013) Discrete Empirical Interpolation Method for Finite Element Structural Dynamics. In: Kerschen G., Adams D., Carrella A. (eds) Topics in Nonlinear Dynamics, Volume 1. Conference Proceedings of the Society for Experimental Mechanics Series, vol 35. *Springer*, New York, NY. DOI: 10.1007/978-1-4614-6570-6_18
- [3] Chaturantabut, S., Beattie, C., Gugercin, S. Structure-preserving Model Reduction for Nonlinear Port-Hamiltonian Systems *arXiv:1601.00527* (2016)
- [4] Barrault, M., Maday, Y., Nguyen, N. C., and Patera, A. T. An “empirical interpolation” method: Application to efficient reduced-basis discretization of partial differential equations, *C. R. Math. Acad. Sci. Paris* (2004) 339: 667–672. DOI: 10.1016/j.crma.2004.08.006
- [5] Farhat, C., Avery, P., Chapman, T., Cortial, J. Dimensional reduction of nonlinear finite element dynamic models with finite rotations and energy-based mesh sampling and weighting for computational efficiency, *International Journal for Numerical Methods in Engineering* (2014) 98(9): 625-662. DOI: 10.1002/nme.4668
- [6] Matthies, H.G., Meyer, M., Nonlinear Galerkin methods for the model reduction of nonlinear dynamical systems, *Computers & Structures* (2003) 81(9): 1277-1286.
- [7] Farhat, C., Chapman, T., Avery, P. Structure-preserving, stability, and accuracy properties of the energy-conserving sampling and weighting method for the hyper reduction of nonlinear finite element dynamic models, *International Journal for Numerical Methods in Engineering* (2015) 102(5): 1077-1110. DOI: 10.1002/nme.4820
- [8] Jain, S., Tiso, P., Haller, G., Exact Nonlinear Model Reduction for a von Karman beam: Slow-Fast Decomposition and Spectral Submanifolds, *submitted*. arXiv:1703.03001v1 (2017)
- [9] Daniel Millán, D., Arroyo, M. Nonlinear manifold learning for model reduction in finite elastodynamics, *Computer Methods in Applied Mechanics and Engineering* (2013) 261: 118-131
- [10] Peharz, R., Pernkopf, F. Sparse nonnegative matrix factorization with ℓ^0 -constraints. *Neurocomputing* (2012); 80:38–46. DOI: 10.1016/j.neucom.2011.09.024
- [11] Jain, S., Tiso, P., Rixen, D.J., Rutzmoser, J.B. A Quadratic Manifold for Model Order Reduction of Nonlinear Structural Dynamics, *Computers & Structures* (2017), 188: 80-94. DOI: 10.1016/j.compstruc.2017.04.005
- [12] Rutzmoser, J.B., Rixen, D.J., Tiso, P., Jain, S. Generalization of Quadratic Manifolds for Reduced Order Modeling of Nonlinear Structural Dynamics, *Computers & Structures* (2017), 192: 196-209. DOI: 10.1016/j.compstruc.2017.06.00

- [13] Lines, L.R., Treitel, S. A review of least-squares inversion and its application to geophysical problems, *Geophysical Prospecting* (1984) 32(2): 159–186. DOI: 10.1111/j.1365-2478.1984.tb00726.x
- [14] van der Maaten, L., Postma, E., van den Herik, J. Dimensionality Reduction: A Comparative Review, TiCC TR 2009?005(2009), Tilburg University
- [15] Ryckelynck D., A priori hyperreduction method: an adaptive approach, *J. Comput. Phys.* (2005) 201(1): 346–366. DOI: 10.1016/j.jcp.2004.07.015
- [16] Jain, S., Model Order Reduction for Non-linear Structural Dynamics, *Master Thesis* (2015), Delft University of Technology. UUID: cb1d7058-2cfa-439a-bb2f-22a6b0e5bb2a
- [17] Mignolet, M.P., Przekop, A., Rizzi, S.A., Spottswood, S.M. A review of indirect/non-intrusive reduced order modeling of nonlinear geometric structures. *J Sound Vib* (2013) 332(10): 2437-2460. DOI: 10.1016/j.jsv.2012.10.017
- [18] Barbič, J., James, D. L. Real-Time Subspace Integration for St. Venant-Kirchhoff Deformable Models. *ACM Trans. Graph.* (2005) 24(3): 982–990. DOI: 10.1145/1073204.1073300
- [19] Everson, R., Sirovich L. Karhunen-Loeve procedure for gappy data. *Journal of the Optical Society of America A* (1995) 12(8):1657?1664. DOI: 10.1364/JOSAA.12.001657
- [20] Haller, G. and Ponsioen, S. Exact model reduction by a slow?fast decomposition of nonlinear mechanical systems, *Nonlinear Dyn.* (2017) 90: 617-647. DOI: 10.1007/s11071-017-3685-9
- [21] Carlberg, K. Bou-Mosleh and Farhat, C. Efficient non-linear model reduction via a least-squares Petrov?Galerkin projection and compressive tensor approximations, *Int. J. Numer. Meth. Engng* (2011); 86: 155-181. DOI: 10.1002/nme.3050
- [22] Carlberg, K., Farhat, C., Cortial, J. and Amsallem D. The GNAT method for nonlinear model reduction: Effective implementation and application to computational fluid dynamics and turbulent flows, *J. Comput. Phys.* (2013), 242:623?647. DOI: 10.1016/j.jcp.2013.02.028
- [23] Chapman, T. , Avery, P., Collins, P. and Farhat, C. Accelerated mesh sampling for the hyper reduction of nonlinear computational models, *Int. J. Numer. Meth. Engng* (2017), 109:1623–1654. DOI: 10.1002/nme.5332
- [24] Rega, G. and Troger, H. Dimension Reduction of Dynamical Systems: Methods, Models, Applications, *Nonlinear Dyn.* (2005), 41: 1?15. DOI: 10.1007/s11071-005-2790-3
- [25] Ding, Q. and Zhang, K. Order reduction and nonlinear behaviors of a continuous rotor system, *Nonlinear Dyn.* (2012), 67: 251?262. DOI: 10.1007/s11071-011-9975-8